NASA TN D-1187

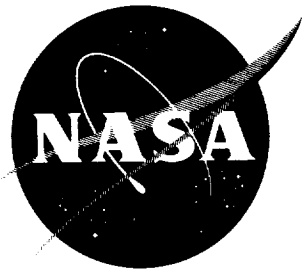

TECHNICAL NOTE

D-1187

EVALUATION OF A HOLLOW, CYLINDRICAL, CONTACT-ION SOURCE

By J. Thomas Kotnik

Lewis Research Center
Cleveland, Ohio

NATIONAL AERONAUTICS AND SPACE ADMINISTRATION

WASHINGTON February 1962

NATIONAL AERONAUTICS AND SPACE ADMINISTRATION

TECHNICAL NOTE D-1187

EVALUATION OF A HOLLOW, CYLINDRICAL, CONTACT-ION SOURCE

By J. Thomas Kotnik

E-1361

SUMMARY

An analysis is presented to determine the ion current that can be obtained by contact ionization of cesium on a cylindrical platinum film having a longitudinal potential gradient imposed on it. Experimental data are shown to compare favorably with the analytical results. The moderately good agreement between the analytical and experimental data would suggest that similar cylindrical sources could be analyzed with the same theoretical model.

An aluminum oxide tube, coated on the inside by a thin film of platinum, was maintained between 1590° and 1725° K for contact ionization of cesium. Cesium vapor was injected at one end of the tube, and the effect on the maximum ion current of a potential gradient applied across the ends of the film was measured.

The current densities obtained were less than 1 ampere per square meter, which would make this device inapplicable for space propulsion.

Heat loss from the cylinder was very great, more than 10^6 electron volts per ion, which produced efficiencies of less than 1 percent.

INTRODUCTION

A practical contact-ionization electrostatic rocket engine must have ion current densities of more than 100 amperes per square meter if reasonable power efficiency and thrust per unit area are to be obtained (ref. 1). As part of the NASA Lewis Research Center's program to investigate various ion sources for use in electrostatic propulsion, a hollow, cylindrical ion source was evaluated experimentally and theoretically.

The investigation was undertaken to determine whether a longitudinal potential gradient on a cylindrical contact-ionization source would increase the exit current density enough to merit its use as an ion source for electrostatic propulsion. The theoretical analysis presented herein is intended to be only an approximate solution to the problem. The complete solution to the space charge flow inside a cylinder has not been

reported, but some previous work has been done on this geometry (refs. 2 and 3).

The cylindrical ionization surface was an evaporated film of platinum. Although tungsten is a more efficient ionization surface, platinum was more convenient to evaporate and produces quite high ionization efficiencies with cesium (ref. 4). A film was used in order to produce a thin conductor with high resistance, so that an appreciable potential could be maintained across it.

The potential gradient applied to the film was varied between 0 and 4000 volts per meter during most of the runs. When the longitudinal potential gradient was eliminated, the data obtained at this time were compared with a previous analysis of a cylindrical ion source with zero potential gradient (ref. 3).

The operating temperature of the film was maintained constant during a run and was varied from 1590° to 1725° K for different runs.

The experimental data obtained are for a tube of 1.23-centimeter radius and 10-centimeter length. The analytical results presented are for a range of tube diameters varying from 1-micron radius to 10-centimeter radius.

SYMBOLS

The following symbols are used in this report:

C	constant of integration
E	potential gradient, v/m
e	particle charge, coulombs
J	ion beam current, amp
J_S	ion beam with no potential gradient applied
ΔJ	ion beam increase due to potential gradient
j	current density, amp/m^2
j_E	emission current density affected by potential gradient
j_S	sheath current density, with no potential gradient applied
Δj	current density increase due to potential gradient

k	Boltzmann's constant, joules/^{o}K
L	length of cylinder, m
m	mass of particle, kg
Q_{cy}	radiation heat loss from inside cylinder, w
$Q_{F \cdot Pl}$	radiation heat loss from a flat plate, w
R	constant, $\frac{4j_E}{\epsilon_0 Er} \sqrt{\frac{m}{2e}}$
r	radius of cylinder, m
T	temperature, ^{o}K
u	particle velocity, m/sec
V	particle potential, v
V_0	potential at $x = 0$, v
x	longitudinal distance along tube axis, m
ϵ	gray-body emittance
ϵ_a	apparent emittance
ϵ_0	permittivity of free space, 8.855×10^{-12}, farad/m
ξ	distance along ionization surface
ρ	charge density at point x, coulombs/m^3
ρ_r	charge density at cylinder radius r, coulombs/m^3
ρ_0	charge density at centerline of cylinder, coulombs/m^3
σ	Stefan-Boltzmann constant, 5.735×10^{-8}, w/m^2-deg^4
$\Phi(x)$	potential difference between tube end potential and beam potential at point x, v
$\varphi(x)$	beam potential at point x, v

Subscripts:

tot	associated with summation of all components
w	associated with tube wall

THEORY

Zero Potential Gradient

The model used to describe the ion source can be considered to be composed of two separate but interrelated processes. The first process to be considered is the ionization off the walls when no potential gradient is applied across the film. It is assumed that the ions leave the surface of the platinum film with a Maxwellian velocity distribution. They establish a radially distributed charge density due to space charge effects. An ion current that depends on the charge density inside the tube will then pass through the screen at the end of the tube, as seen in sketch (a), and will be referred to as the sheath current.

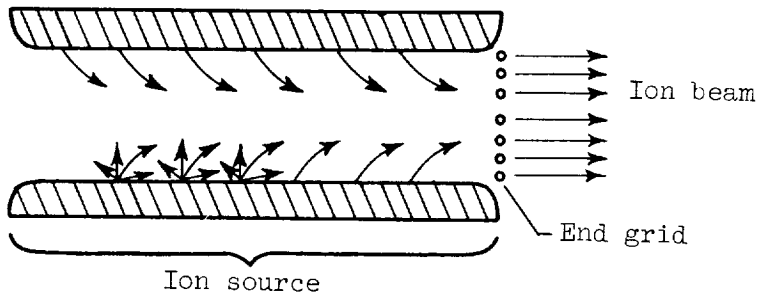

(a)

The charge density inside the cylinder can be obtained by the solution of Poisson's equation as shown in reference 5. Reference 3 gives the maximum current to be expected as related to the film temperature as

$$J_S = \pi r^2 \sqrt{\frac{kT}{2\pi m}} \sqrt{\rho_0 \rho_R} \qquad (1)$$

in which $\sqrt{kT/2\pi m}$ represents the arithmetical average velocity divided by 4 and $\sqrt{\rho_0 \rho_r}$ is an average charge density over the tube cross section. The ion density inside the tube rapidly decreases toward the tube axis; this causes the exit beam to be in the form of a thin sheath along the tube surface.

Figure 1 shows curves of the theoretical current density expected for cesium ionized on platinum from a cylindrical source without a longitudinal potential gradient, using the model described, for various radii

and wall temperatures. The experimental test was conducted with a cylinder having a radius of 1.23×10^{-2} meter, which is represented on the right side of the figure. Figure 2 is the same family of curves as figure 1 except that cesium is ionized on tungsten, which would allow a higher current density for the same operating conditions. In both figures 1 and 2, it can be seen that a decrease in tube radius at constant wall temperature, or an increase in wall temperature at a constant tube radius, results in an increase in current density from the tube. In both figures, at the lower wall temperature, the current density levels off as the radius is decreased; this happens when the tube becomes temperature-limited instead of space-charge-limited. The charge density in the center of the tube then approaches the charge density at the wall.

One-Dimensional Flow With a Potential Gradient

The second process consists of an increase in ion flow toward the end of the tube because of an externally applied longitudinal potential gradient. A potential $\varphi(x)$ will be established in the center of the tube which is greater than the wall potential at any particular cross section because of ion flow (see sketch (b)). This beam potential $\varphi(x)$ is equal to the boundary potential at $x = 0$, where ions have not been formed, and at $x = L$, where the end grid forces the potential $\varphi(x)$ to equal $(V_0 - LE)$, the exit potential.

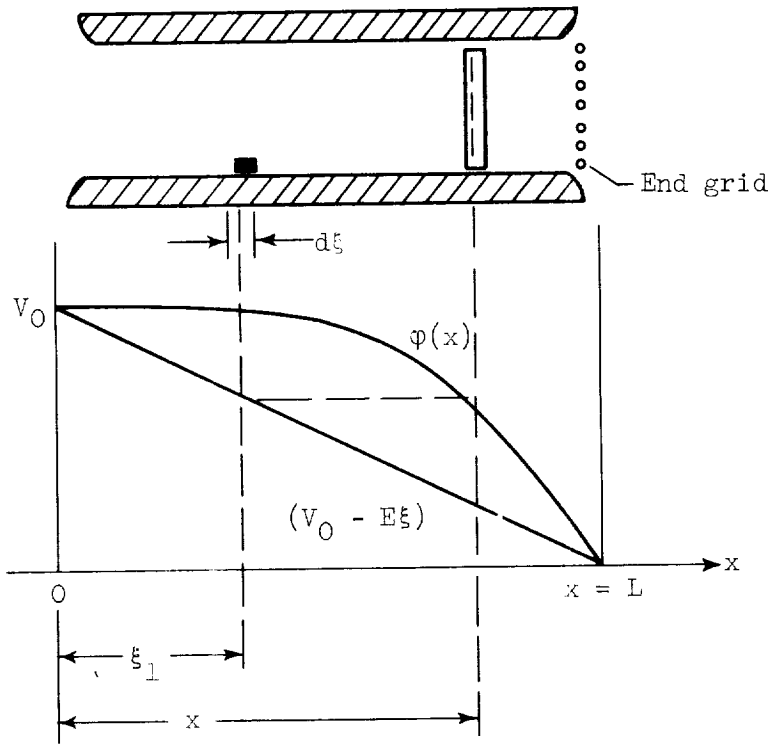

(b)

When a potential gradient is applied to the tube, ions are emitted from the wall at position ξ with potential energy $V = V_0 - E\xi$ relative to the end of the cylinder. Because of space charge effects, the potential φ near the center of the tube is higher than at the wall. To estimate this potential, it is necessary to estimate the space charge distribution along the tube. This is done by assuming that the potential φ is about constant across the tube, except in a thin surface sheath, wherein the potential diminishes from φ to V.

The ions emitted between $\xi = 0$ and ξ_1 will contribute to the space charge at station x, where ξ_1 is the station at which the wall potential is equal to the center potential station x. Thus,

$$u(\xi,x) = \left[\frac{2e}{m} V_0 - E\xi - \varphi(x)\right]^{1/2} \tag{2}$$

The current at x due to emission at an element of length $d\xi$ is

$$dJ = j_E \cdot 2\pi r \, d\xi \tag{3}$$

where j_E is the emission current density, which is assumed constant for a given wall temperature. The space charge density at x due to these ions is

$$d\rho(\xi,x) = \frac{dJ}{\pi r^2 u(\xi,x)} \tag{4}$$

Combining equations (2), (3), and (4) and integrating from $\xi = 0$ to $\xi = \xi_1$ yield

$$\rho(x) = \int_0^{\xi_1} \frac{2j_E}{r\sqrt{\frac{2e}{m}}} \frac{d\xi}{\left[V_0 - \varphi(x) - E\xi\right]^{1/2}}$$

$$= -\frac{4j_E}{rE\sqrt{\frac{2e}{m}}} \left[V_0 - \varphi(x) - E\xi_1\right]^{1/2} - \left[V_0 - \varphi(x)\right]^{1/2} \tag{5}$$

But

$$\xi_1 = \frac{V_0 - \varphi(x)}{E}$$

Hence,

$$\rho(x) = \frac{4j_E}{r\sqrt{\frac{2e}{m}}\,E}\,\Phi(x) \tag{6}$$

where $\Phi(x) = V_0 - \varphi(x)$. From Poisson's equation in one dimension,

$$\frac{d^2\varphi}{dx^2} \equiv -\frac{d^2\Phi}{dx^2} = -\frac{\rho}{\epsilon_0} = -R\Phi^{1/2} \tag{7}$$

where

$$R = \frac{4j_E}{\epsilon_0 Er}\sqrt{\frac{m}{2e}}$$

Multiplying both sides by $2(d\Phi/dx)$ and integrating yield

$$\left(\frac{d\Phi}{dx}\right)^2 = \frac{4}{3}R\Phi^{3/2} + C_1 \tag{8}$$

With space-charge-limited conditions at $x = 0$ assumed,

$$\Phi_0 = \left(\frac{d\Phi}{dx}\right)_0 = 0; \qquad \text{then} \quad C_1 = 0$$

Integrating again by the separation of variables gives

$$4\Phi^{1/4} = \sqrt{\frac{4}{3}R}\,x \tag{9}$$

where the integration constant is again zero for space-charge-limited conditions. Replacing R and squaring both sides yields

$$16\Phi^{1/2} = \frac{4}{3}\left(\frac{4j_E}{\epsilon_0 kr}\right)\sqrt{\frac{m}{2e}}\,x^2 \tag{10a}$$

At $x = L$, $\Phi = V_0 - \varphi(x)$; so that the current density that can be emitted from the wall can be written

$$j_E = 3\epsilon_0 Er\sqrt{\frac{2e}{m}}\,\frac{V_0^{1/2}}{L^2} \tag{10b}$$

The additional current due to the potential gradient is the emitted current density times the wall area $2\pi rL$:

$$\Delta J = 2\pi rLj = 6\pi r^2 \epsilon_0 EL \sqrt{\frac{2e}{m}} \frac{V_0^{3/2}}{L^2} \tag{11}$$

In this case $E = (V_0/L)$ and $\Delta j = (\Delta J/2r^2)$, so that

$$\Delta j = 6\epsilon_0 \sqrt{\frac{2e}{m}} \frac{V^{3/2}}{L^2} \tag{12}$$

When equation (12) is compared with the theoretical Child's law maximum current from a plane diode of the same cross-sectional area and accelerator space equal to the tube length, it can be seen that 13.5 times more current can be obtained by using the tube rather than a plane diode because of the potential gradient.

To find the total theoretical current density from the cylindrical source investigated, the value of current density obtained because of the potential gradient would be superimposed on the current density obtained from the consideration of thermal energy:

$$j_{tot} = \sqrt{\frac{kT}{2\pi m}} \sqrt{\rho_0 \rho_r} + 6\epsilon_0 \sqrt{\frac{2e}{m}} \frac{\Delta V^{3/2}}{x^2} \tag{13}$$

Power Losses

The power loss due to radiation from a long cylinder can be calculated by the method given in reference 6:

$$Q_{cy} = \int_0^L \sigma T^4 \frac{\epsilon}{1 - \epsilon} (1 - \epsilon_a) 2\pi r \, dx \tag{14a}$$

$$Q_{cy} = \sigma T^4 \frac{\epsilon}{1 - \epsilon} 2\pi r \left[L - \int_0^L \epsilon_a \, dx \right] \tag{14b}$$

Since apparent emittance ϵ_a is given in terms of $x/2r$ in reference 6, the variable is changed from x to $x/2r$, and the radiation heat-loss equation becomes

$$Q_{cy} = \sigma T^4 \left(\frac{\epsilon}{1 - \epsilon}\right) 4\pi r^2 \left[\frac{L}{2r} - \int_0^{\frac{L}{2r}} \epsilon_a \, d\left(\frac{x}{2r}\right)\right] \tag{15}$$

The total emittance of the platinum film is taken to be 0.3, as the film on the aluminum oxide tube was a dull gray in texture. From the value of ϵ_a as found in reference 6, equation (15) can be numerically integrated to obtain:

$$Q_{cy} = 0.76 \, \sigma\pi T^4 r^2 \tag{16}$$

from one open end of the cylinder.

When compared with a flat plate of the same emittance and area equal to the cross-sectional area of the tube, the effective emittance of the cylinder is found to be 2.46 times greater than that of the plane plate. Figure 3 gives the relation of the ratio $Q_{cy}/Q_{F \cdot Pl}$ as a function of emittance and the ratio $L/2r$; the location of the experimental tube point is shown at $\epsilon = 0.3$ and $L/2r = 4.07$. It should be noted that the curves would go to zero at $L/2r = 0$, as the cylinder is bottomless. If a bottom were in the cylinder, the curves would converge at $Q_{cy}/Q_{F \cdot Pl} = 1$.

The theoretical radiation power loss from the film surface, out both ends of the experimental tube, is shown in figure 4 as a function of the film temperature.

APPARATUS

A cutaway view of the apparatus used in this investigation is shown in figure 5. In general, the cesium is heated inside the vaporizer, and the vapor is emitted into the tube through a perforated cap. The vapor flows onto the surface of the tube, being ionized by the platinum film. The ions move up the tube because of the potential gradient and thermal energy, flow through the grid across the top end of the tube, and are accelerated into a grounded cold trap.

Ceramic Tube

To provide a thin-walled cylinder, platinum was evaporated on the inner surface of a high-purity (99.5+ percent) aluminum oxide tube. The high-purity tubing was necessary to prevent contamination of the evaporated film at high temperatures. The tube was approximately 10 centimeters long with a 2.46-centimeter inside diameter and a wall thickness of 0.35 centimeter (see fig. 5). The inside wall edges were rounded, and the film was extended over the ends of the tubing. The resistance of the platinum film was kept above 10,000 ohms.

Electrical contact with the platinum film was established by clamping stainless-steel rings against the top and bottom of the tube with leads tack-welded to the rings. A grid of 5-mil-diameter tungsten wire spaced 50 mils apart was located on the top ring to prevent the accelerator potential from affecting the potential within the tube. The rings were held under pressure by three sapphire-ball insulators and end plates.

Heating

A resistance heater composed of a winding of 25-mil tantalum wire around the alumina tube was used to produce the desired temperature. The tube was surrounded by four heat shields. The inside shield was made of 20-mil tantalum, and the outer three were made of 16-mil stainless steel. Holes were notched in the shields to allow the electrical and thermocouple leads to extend out.

End Plates

Both end plates were made of 0.635-centimeter-thick stainless steel and were 8.9 centimeters in diameter. A tapered hole in the center of the top plate allowed an accelerator grid mounted on a tapered ring to be placed over the end screen of the tube. The grid was made of 25-mil tungsten wire spotwelded to the bottom of the tapered ring with 250-mil spacing between the wires. The accelerator grid was 1.11 centimeters from the cylinder and grid. The accelerator grid, with a negative potential applied, also served as a screen to prevent the back streaming of electrons from the cold-trap target.

The accelerator was operated mainly at a potential which ensured that it was well above the critical Child's law potential for the expected current and the set accelerator distance. The voltage was set to optimize the current to the cold trap, which would minimize the accelerator impingement. No attempt was made to record the accelerator impingement current. Impingement might reasonably be assumed to amount to 10

percent of the beam current or less, depending on the accelerator and end grid alinement. Accounting for this impingement would not affect the power efficiency appreciably.

The bottom end plate was similar to the top plate. The four heat shields all rested on the bottom end plate.

Vaporizer

The vaporizer was made of copper, while the vaporizer cap was made of stainless steel. The vaporizer reservoir was 4.44 centimeters long and 0.91 centimeter in diameter, and it was wrapped with a copper cooling coil through which water flowed to hold the vaporizer at the desired temperature. The vaporizer was heated by radiation and conduction from the ceramic tube and the vaporizer cap. Some contamination of the cesium was believed to occur, as it was sometimes necessary to overheat the vaporizer to get an initial substanital increase in flow rate.

The vaporizer cap was 8.9 centimeters long and had eight equally spaced 0.218-centimeter-diameter holes at the top end of the cap side wall. The holes were tilted upward to a 45° angle with the horizontal and acted as a distributor.

INSTRUMENTATION

A schematic with the ratings of the power supplies required during operation of the source is shown in figure 6. The ion current to the cold trap was observed by means of a triple-range microammeter through which the cold trap was grounded. The a-c power to the tantalum wire heater was observed with a 30-ampere ammeter and a 150-volt voltmeter; the power was supplied through a variable autotransformer.

The potentials of the film and accelerator were observed with a portable volt-ohm meter. No attempt was made to record the currents to the film and the accelerator grids.

A Chromel-Alumel thermocouple mounted inside the body of the copper vaporizer was used to observe the temperature of the propellant inside the vaporizer. A platinum - 10% rhodium-platinum thermocouple was placed against a midpoint on the outside wall of the aluminum oxide tube and was monitored with a calibrated meter, making it possible to observe the temperature of the ceramic tube wall.

Because of the temperature gradient present in the tube wall, a correction was applied to the observed temperature to obtain the film temperature. The correction was calculated by estimating the film temperature and using figure 4 to obtain the power loss due to radiation. Using

this power loss, a thermal conductivity of 0.045 (cal)(cm)/(sec)(cm^2)(^oC), and knowing the outside wall temperature, it was possible to calculate an inside wall temperature. This was an iterative process and was repeated until the estimated and calculated inside wall temperatures agreed within 1° C. The calculated temperature drop through the wall of the tube varied from 79° to 109° C.

The ion current was measured through a microammeter to ground from the isolated cold trap. With adequate acceleration-deceleration to prevent the back streaming of electrons, the microammeter reading was believed to give a reliable indication of the ion current. The screen grids probably intercepted about 10 percent of the ion current, but this would not be enough to change the results appreciably.

Vacuum Facility

The ion source was installed in a vertically mounted glass cylinder shown in figure 7, which measured 18 inches in diameter and 36 inches in height.

The cold-trap target was 12 inches in diameter and 9 inches long, was made of 1/8-inch-thick copper, and was wrapped with nine turns of 1/2-inch copper tubing for liquid-nitrogen cooling.

Water cooling was used on a copper jacket around the assembled ion source to prevent the glass from becoming hot. A water cooling line was also used to control the temperature of the vaporizer. The vaporizer cooling water passed through plastic tubing at both the inlet and exit to isolate the vaporizer from ground.

Procedure

The loading of the vaporizer was accomplished by first lowering the temperature of vaporizer chamber and the cesium capsule to liquid-nitrogen temperature while the ion source was disassembled. The capsule was then placed inside the vaporizer, and the glass ampule was broken. At liquid-nitrogen temperature, the cesium was relatively nonreactive and could be handled safely. Once the ampule was broken, the ion source was assembled and the glass cylinder was evacuated as quickly as possible.

The vaporizer was kept as cold as possible, while the aluminum oxide tubing was heated to the proper ionization temperature range and degassed. After the pressure had reached the 10^{-7}-millimeter-mercury range, the vaporizer was allowed to heat and the potentials were set to the desired values to obtain data. This usually required an hour of pumping.

After the heating of the vaporizer to obtain the initial current surge, the vaporizer was cooled and the current allowed to decrease. Because of difficulties in setting a precise vaporizer temperature, it was allowed to come to equilibrium near a predetermined value. The temperature of the tube was slowly raised while the current was recorded. At a certain wall temperature, the current would peak and then level off, which indicated that the current was limited by the temperature of the vaporizer. The wall temperature was then lowered until the cold-trap current again decreased. Immediately the wall temperature was raised about 20° to just restore the temperature-limited current. The data for current increase due to the longitudinal potential gradient were then obtained. The vaporizer temperature was raised, and the process was repeated at a different vaporizer temperature and corresponding wall temperature. It was believed that this procedure would minimize the flow rate of neutrals inside the cylinder.

COMPARISON OF THEORY AND EXPERIMENTAL DATA

The ion current to the cold trap is shown in figure 8 as a function of the potential gradient inside the tube. Several runs were made during which the potential gradient was varied between 500 to 4000 volts per meter, but the potential gradient was never eliminated completely. It was assumed that the curve could be extended over to the zero gradient axis by a linear extrapolation. Later runs were made in which the potential gradient was eliminated, and these runs proved the validity of the linear extrapolation. It can be seen that increasing the axial potential gradient inside the tube produced some increase in current for a particular wall temperature.

Figure 9 compares the experimental data with the theoretically predicted current increase due to a longitudinal potential gradient. For each run, these data were obtained by subtracting the sheath current J_S, found with the gradient reduced to zero, from the cold-trap current for the varying potential gradient as found in figure 8. According to the theoretical model previously described, a current increase 13.5 times that calculated using Child's law was predicted. For emitter temperatures of 1590°, 1675°, and 1725° K, theory and experiment agree within an order of magnitude. This current increase due to the potential gradient is small compared with the sheath current, particularly at high temperatures. There is an increase in current with each increase in wall temperature, which suggests that some factor dependent on temperature needs to be included in the theoretical model.

In figure 10, the theoretical current is plotted for zero potential gradient along the tube. Although there is an order-of-magnitude correlation between the theory and the experiment, the current was found to

increase with wall temperature more rapidly than theory predicts. This would be the situation if the slope of the current - critical temperature curve for cesium on platinum given in figure 11 is not correct.

The current - critical temperature relation,

$$\log_{10} j = 11.3 - (14{,}300/T) \qquad (17)$$

is an important factor in determining the temperature-limited current density of cesium ions from a platinum surface. This equation was obtained from the datum point that can be found in reference 4. The curve was run through the one point, as marked in figure 11 at about 1180° K, parallel to the current - critical temperature relation for cesium on tungsten that can be found in reference 7. Because the datum point used was in the lower temperature range, an error in the slope of the relation would be more noticeable at higher temperatures. It is doubtful that the difference between the theory and the experimental datum point at 1725° K could be completely explained in this manner, but it would greatly decrease the difference.

Another factor that would cause the experimental data to exceed the theoretical data would be the presence of the vaporizer cap and the fact that this was a cylinder of finite length. They would tend to diminish the space charge effect, although the use of an end grid would compensate for the finite length.

When all the assumptions involved in the theoretical calculations are considered, order-of-magnitude correlation between the experimental and theoretical data is considered quite satisfactory.

The heating power required to obtain 1590° K was 800 watts, while for 1675° K, the power required was 1010 watts. This power loss overshadows any other power losses that might be present, such as accelerator impingement losses or nonuniform velocities of the ions in the beam.

The heat loss from the source is not all due to radiation from the inside of the tube. During operation of the tube, many supporting parts were observed glowing a dull red. Even with the heat shielding, it was obvious that there was a substantial heat loss from the outside surface of the tube. Conduction losses were reduced to a minimum by using ball insulators to support the tube; this probably accounted for a small portion of the power loss. It can be safely assumed that radiation from the heating winding and the outside tube wall accounted for 50 percent or more of the power loss, since conduction losses are small and radiation losses are calculated and shown in figure 4.

This large power loss due to heating would cause the device to have extremely low power efficiencies, much less than 1 percent for the data obtained.

Figure 12 shows the energy required to ionize an atom with this cylindrical source. The solid-line curve that extends from 1300° to 1900° K is the value obtained by using the theoretical radiation power loss from both ends of the tube and the theoretical current with a 3000-volt-per-meter potential gradient present. Although radiation loss from the vaporizer end of the tube would be lower than the value obtained for an open end, the open-end radiation loss was doubled to account for other losses such as conduction and imperfect shielding.

The curve with data points circled represents the actual power loss divided by the actual experimental current obtained with a 3000-volt-per-meter potential gradient. The third curve, with the square data points, represents the energy per ion using the theoretical radiation power loss divided by the actual currents obtained experimentally.

CONCLUSIONS

An analytical and experimental study has been made of the current density obtainable from a hollow, cylindrical ion source, in which contact ionization of cesium was produced on the inner wall of the cylinder. Although the analysis was based on a simple one-dimensional model, experimental results agreed within an order of magnitude with the theoretical results. It was found that current densities obtainable from the end of the cylinder are about an order of magnitude greater than those obtainable from a plane diode for which the separation of the electrodes is equal to the tube length. However, the current density is only a few percent of that obtainable from a plane diode with spacing between electrodes equal to that between the ends of the tube and the accelerator grid. Only a slight increase in current density was attained by applying a longitudinal potential gradient to the cylinder. Consequently, the hollow, cylindrical ion source investigated has no potential usefulness for electrostatic rockets. To achieve adequately high current density, it is necessary to have cylinder diameters of the order of magnitude of a few microns.

Lewis Research Center
National Aeronautics and Space Administration
Cleveland, Ohio, October 27, 1961

REFERENCES

1. Mickelsen, William R.: Electric Propulsion for Space Flight. Aerospace Eng., vol. 19, no. 11, Nov. 1960, pp. 6-11; 36.

2. Kirstein, P. T., and Kino, G. S.: Solution to the Equations of Space-Charge Flow by the Method of the Separation of Variables. Jour. Appl. Phys., vol. 28, no. 12, Dec. 1958, pp. 1758-1767.

3. Reynolds, Thaine W., and Kreps, Lawrence W.: Gas Flow, Emittance, and Ion Current Capabilities of Porous Tungsten. NASA TN D-871, 1961.

4. Datz, Sheldon, and Taylor, Ellison H.: Ionization of Platinum and Tungsten Surfaces. I - The Alkali Metals. Jour. Chem. Phys., vol. 25, no. 3, Sept. 1956, pp. 389-394.

5. Weymann, H. D.: Electron Density Distribution in a Cylinder. Inst. Fluid Dynamics and Appl. Math., TN BN-214, Univ. Maryland, July 1960.

6. Sparrow, E. M., and Albers, L. U.: Apparent Emissivity and Heat Transfer in a Long Cylindrical Hole. Jour. Heat Transfer, vol. 82, no. 3, Aug. 1960, pp. 253-255.

7. Reynolds, Thaine W., and Childs, J. Howard: A Graphical Method for Estimating Ion-Rocket Performance. NASA TN D-466, 1960.

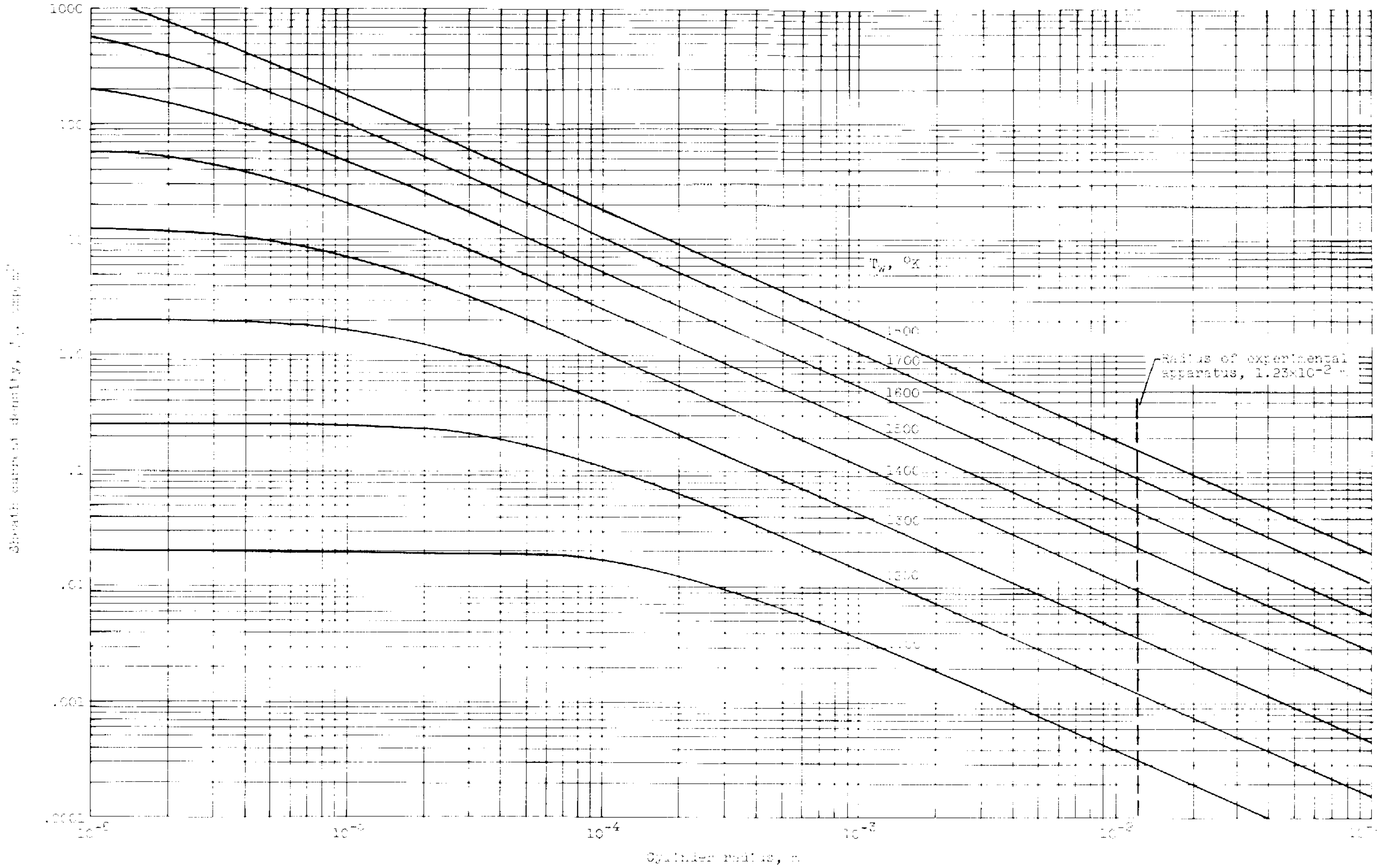

Figure [illegible]. - Maximum current density from hollow platinum cylinder used for contact ionization of cesium. No impressed longitudinal potential gradient.

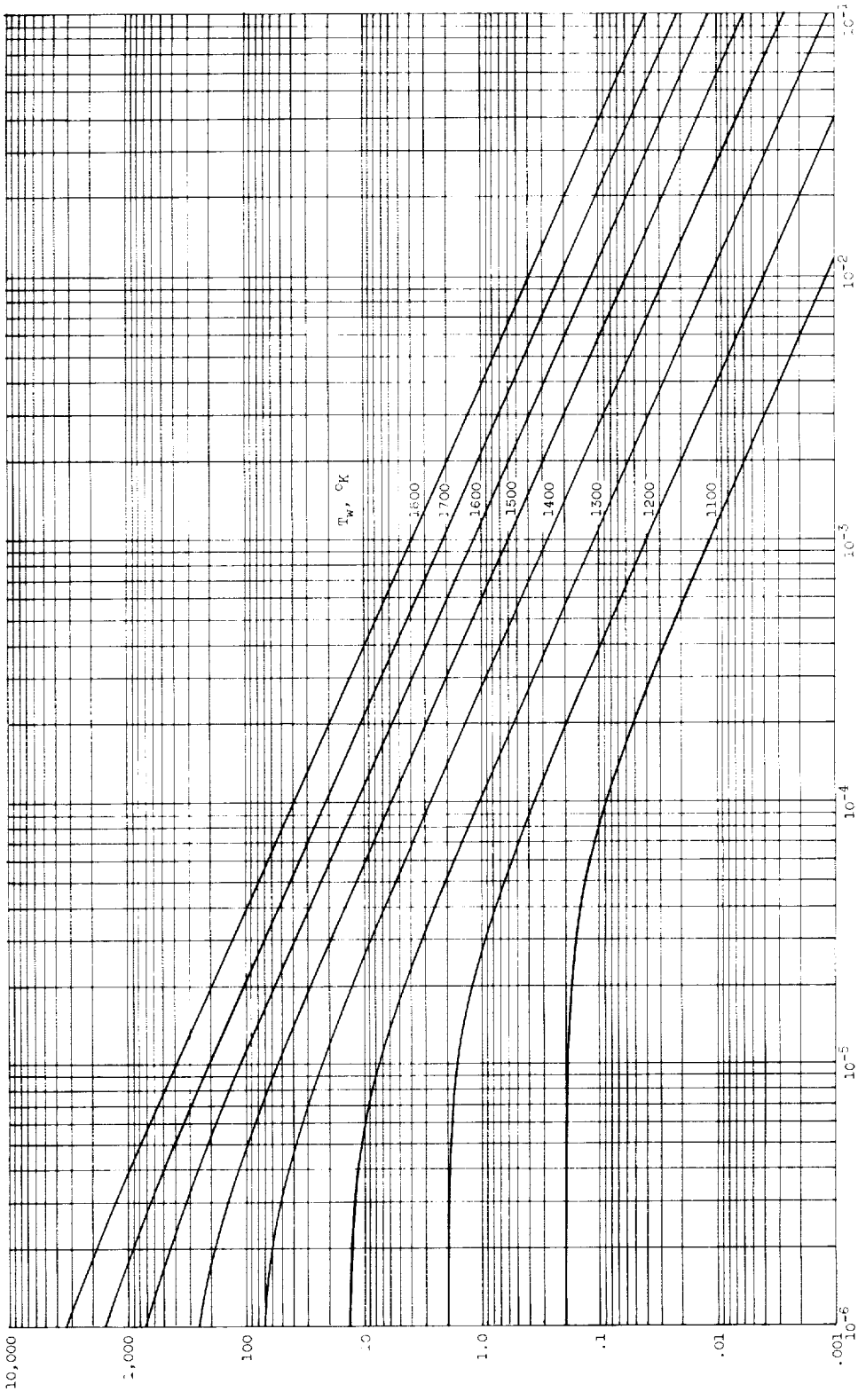

Figure 2. - Maximum current density from hollow tungsten cylinder used for contact ionization of cesium. No impressed longitudinal potential gradient.

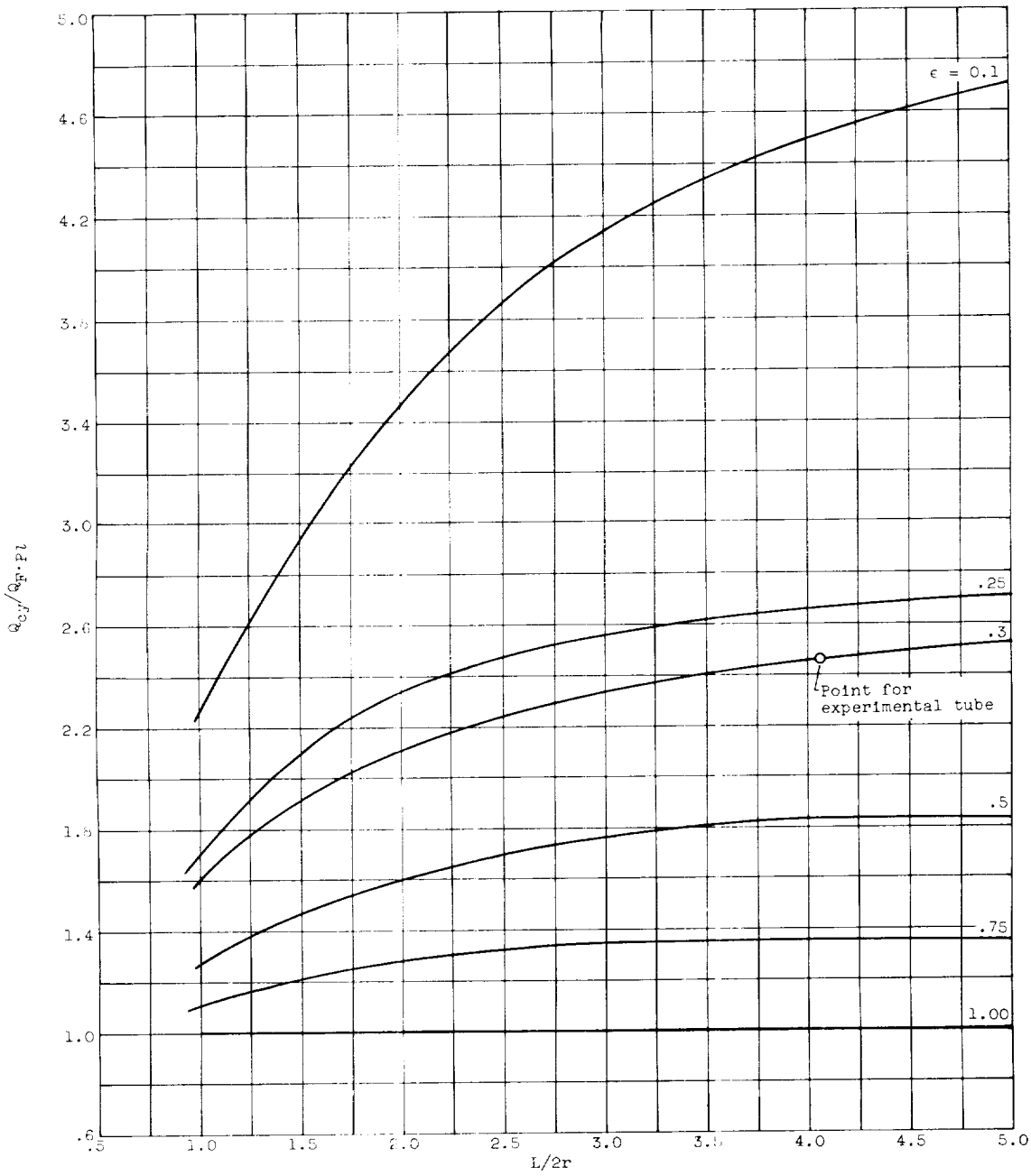

Figure 3. - Ratio of radiant heat loss from a cylinder to the radiant heat loss of a flat plate of the same emittance and with the flat-plate surface area equal to cylinder cross-sectional area.

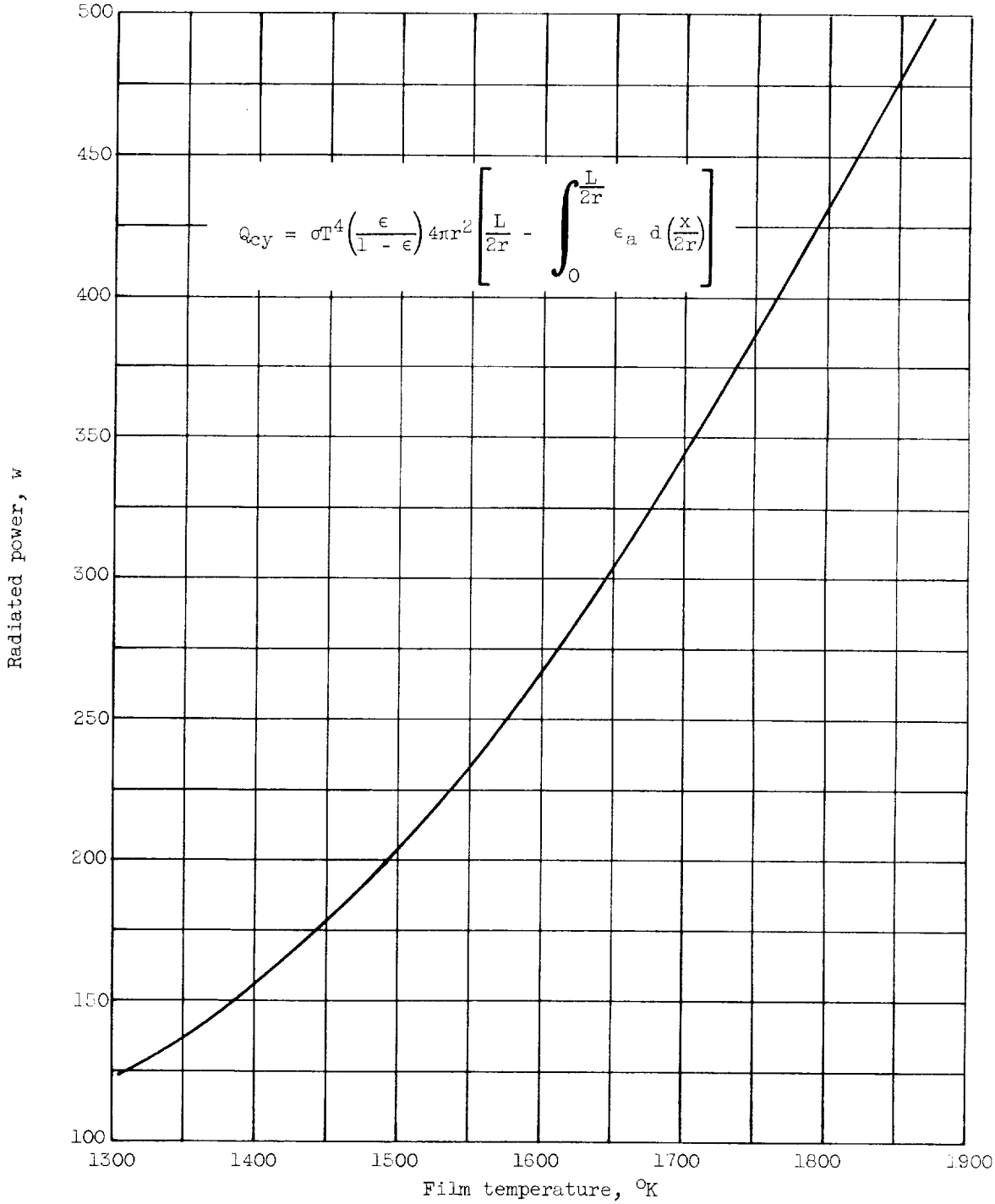

Figure 4. - Theoretical radiation power loss of cylindrical ion source. Length of cylinder, 10 centimeters; emittance, ϵ, 0.3; radius, 1.23×10^{-2} meter; length, 0.10 meter.

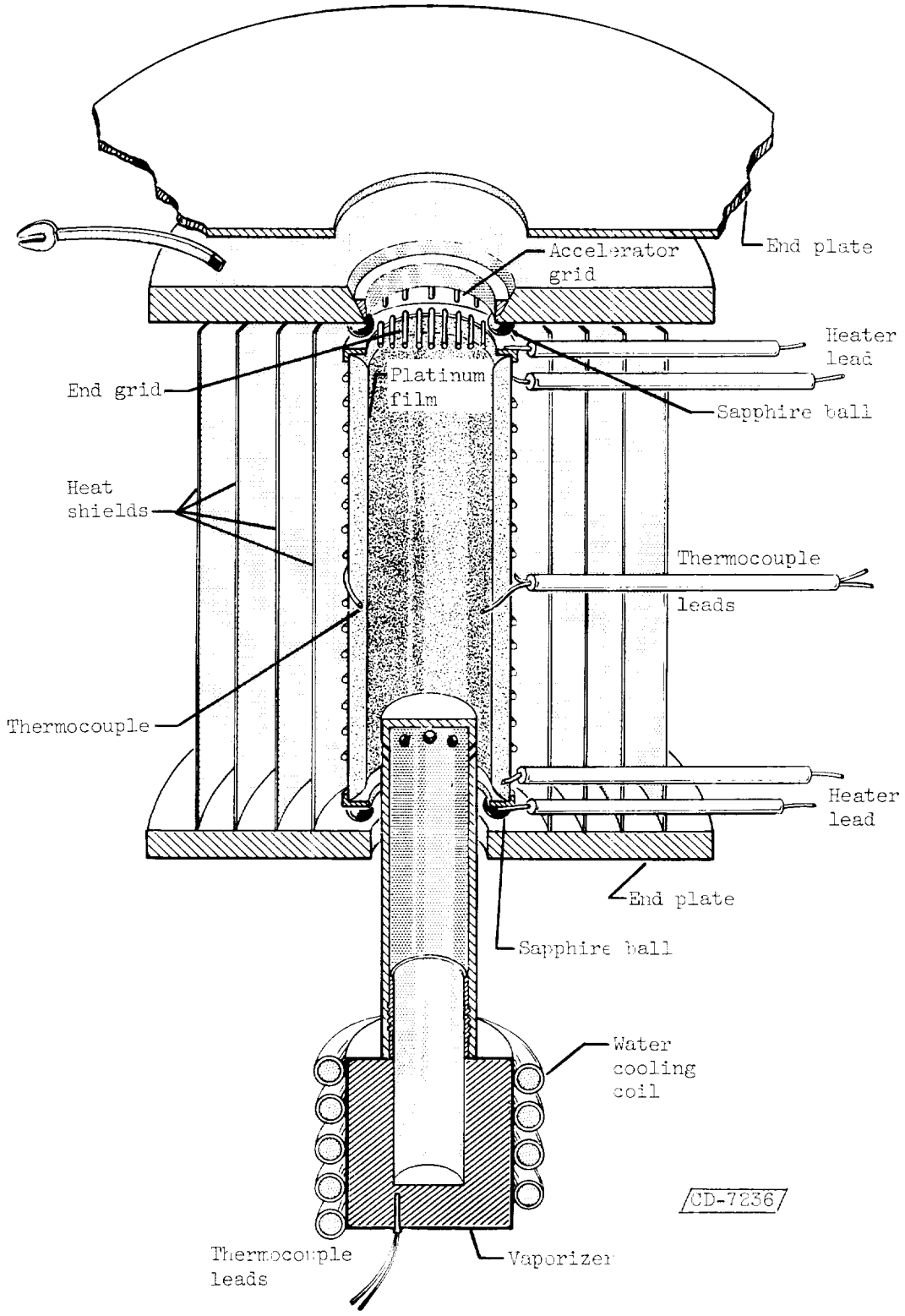

Figure 5. - Platinum film ion source.

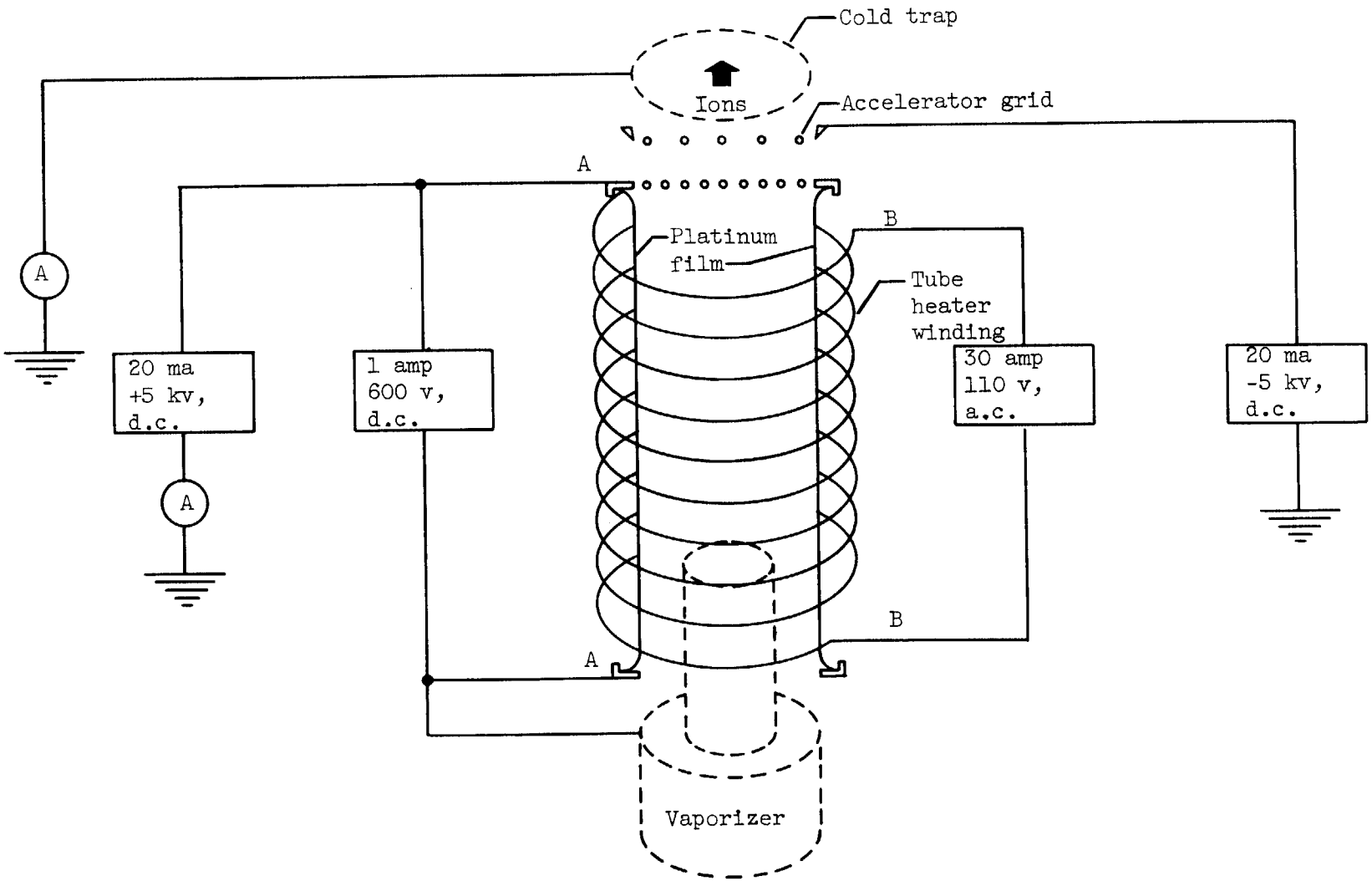

Figure 6. - Power supplies used in experiment.

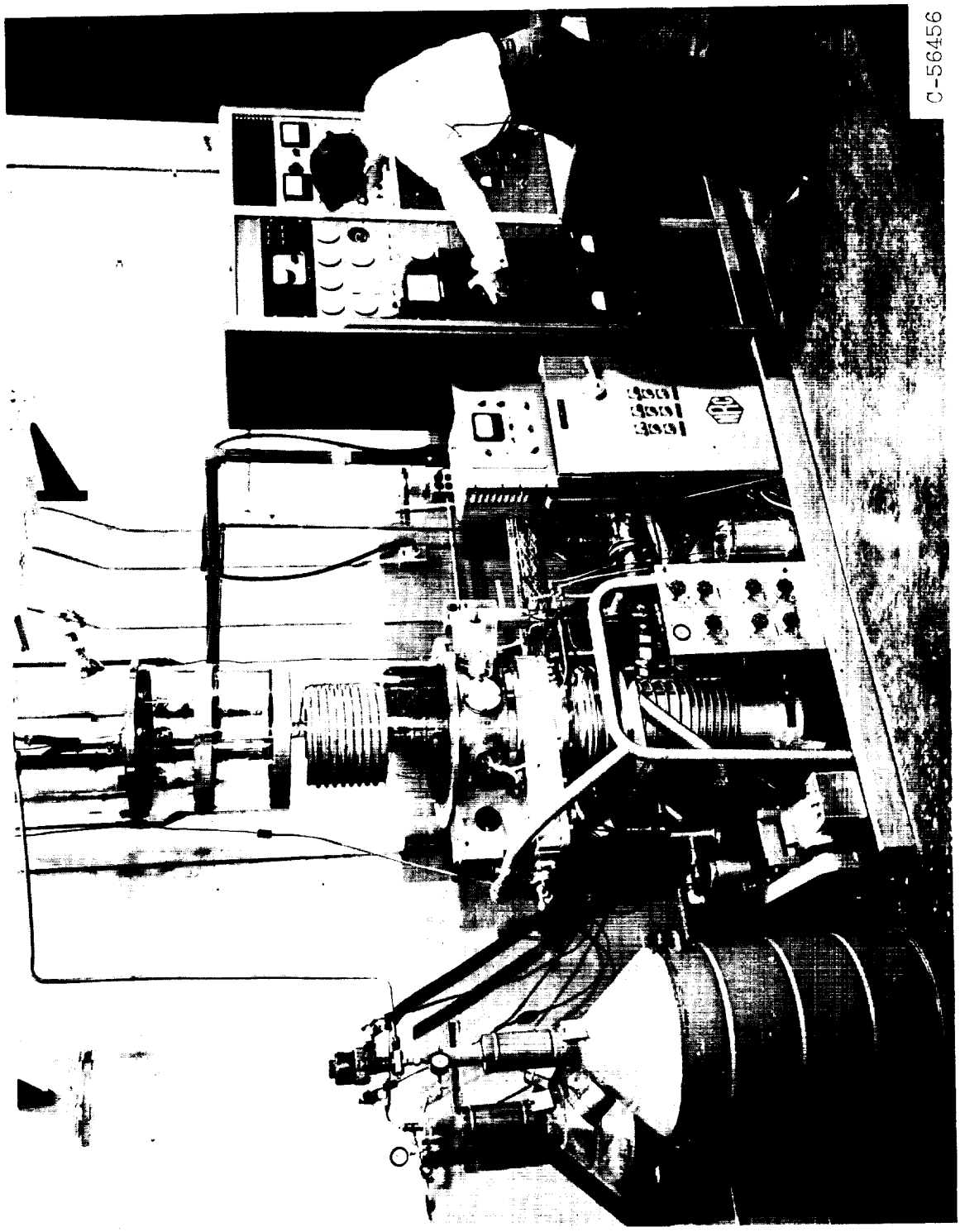

C-56456

Figure 7. - Vacuum facility.

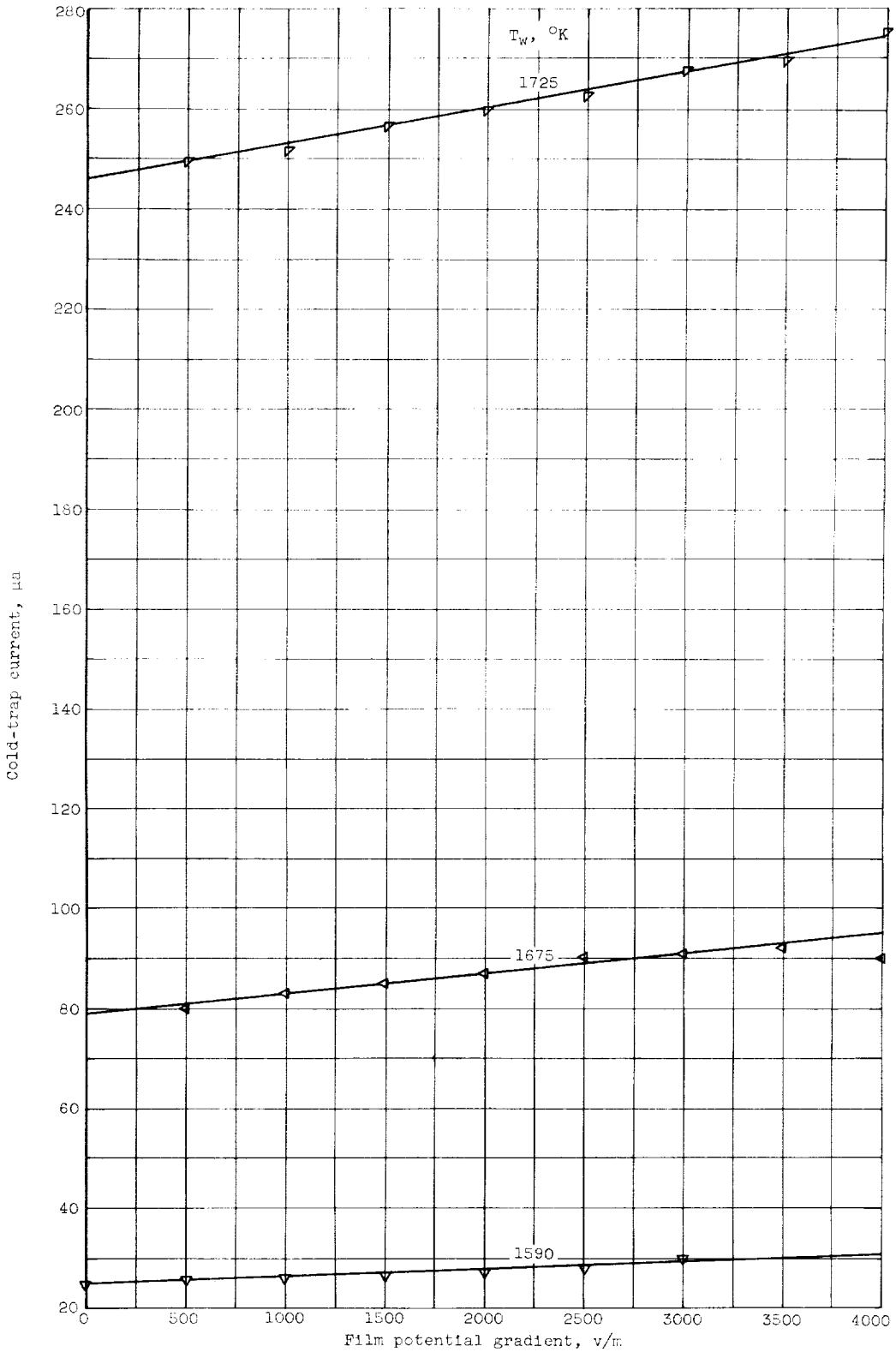

Figure 6. - Experimental data of current to cold trap as film gradient is varied.

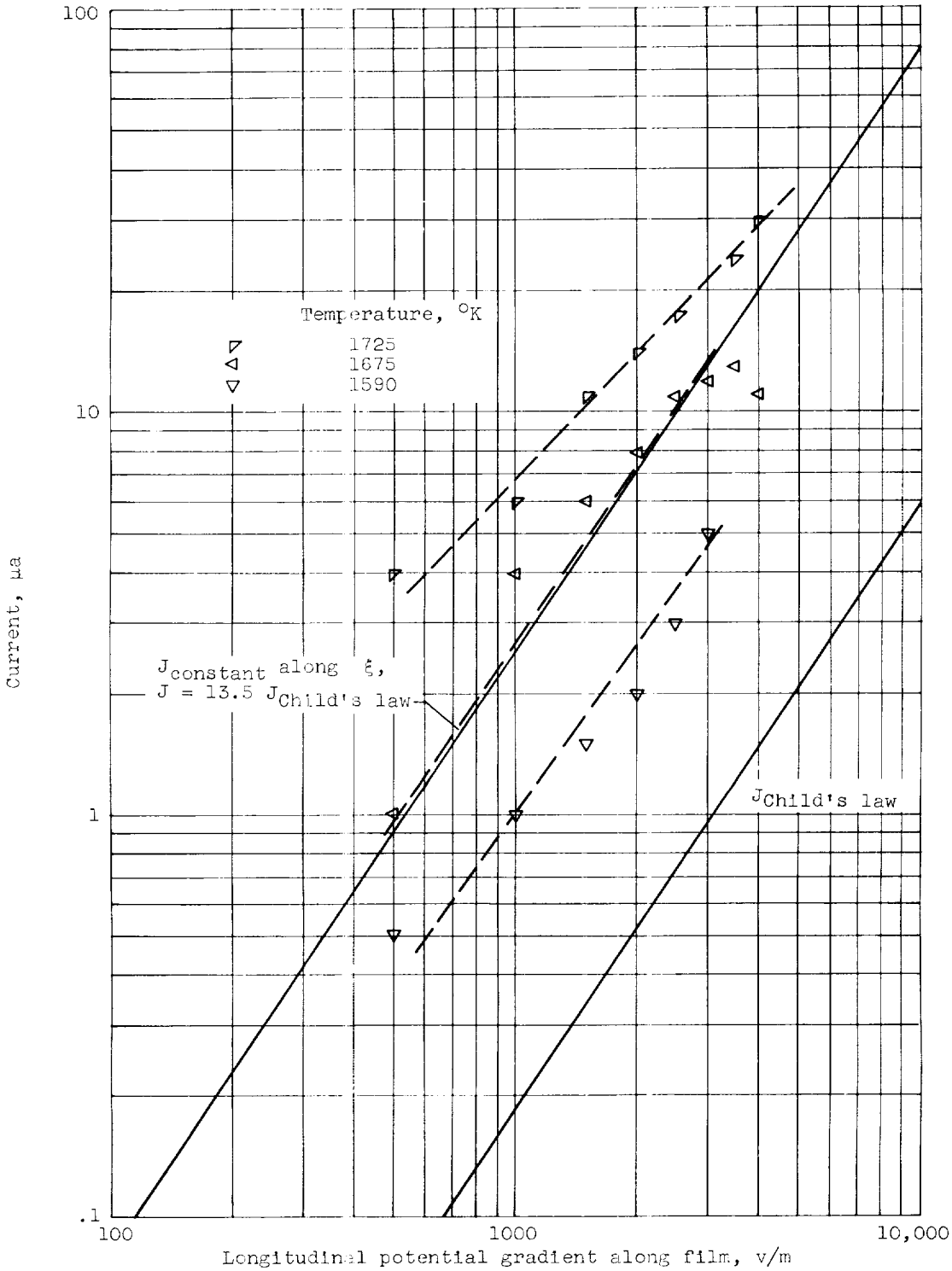

Figure 9. - Comparison of theoretical and experimental ion current; increase due to a longitudinal potential gradient. Propellant, cesium; $J_{Child's\ law}$, $1.8 \times 10^{-10}\ V^{3/2}$; tube length, 10 centimeters; tube cross-sectional area, 4.76 square centimeters.

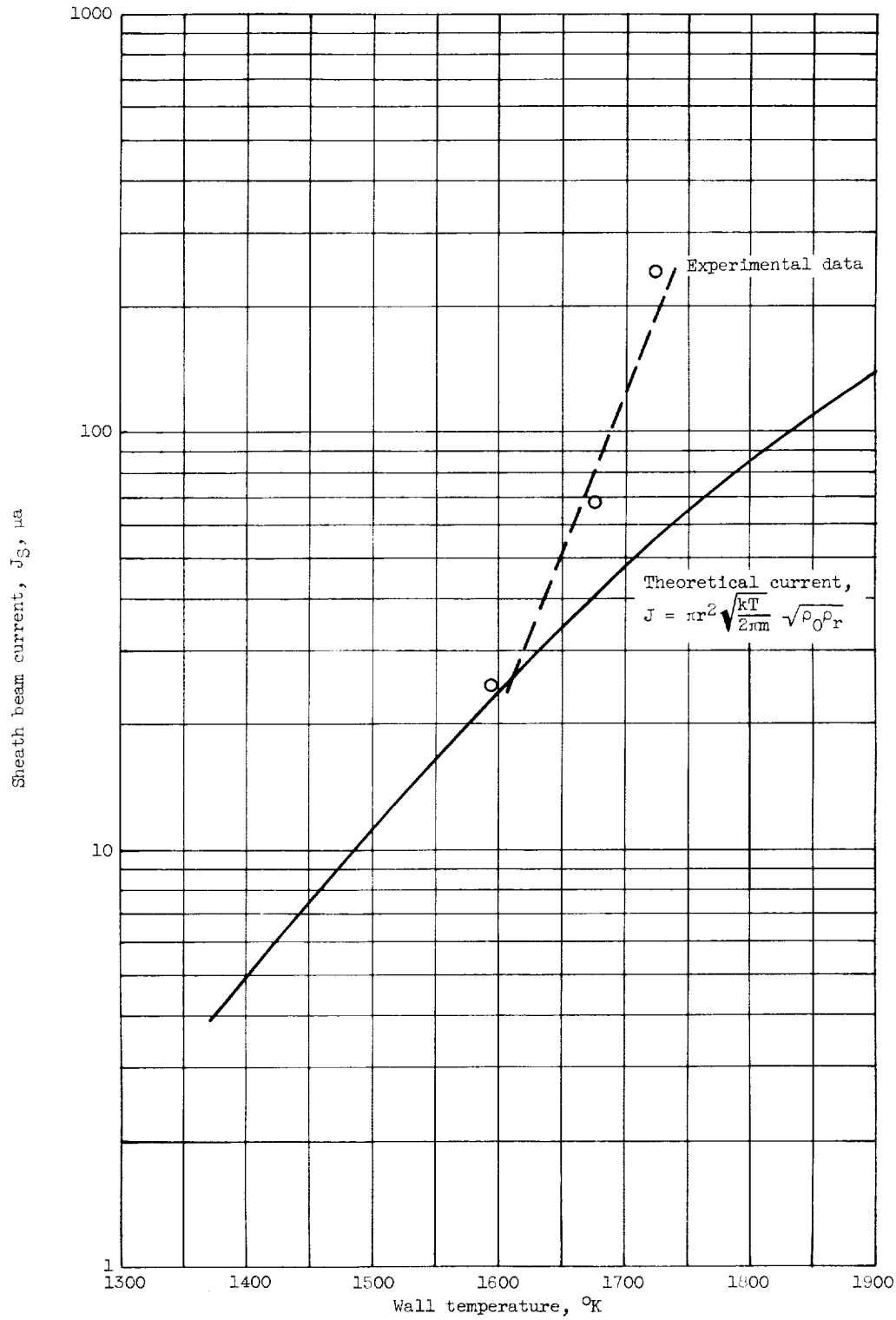

Figure 10. - Comparison of theoretical and experimental ion beam currents with zero potential gradient applied. Radius of tube, 1.23×10^{-2} meter; propellant, cesium; length of tube, 0.10 meter.

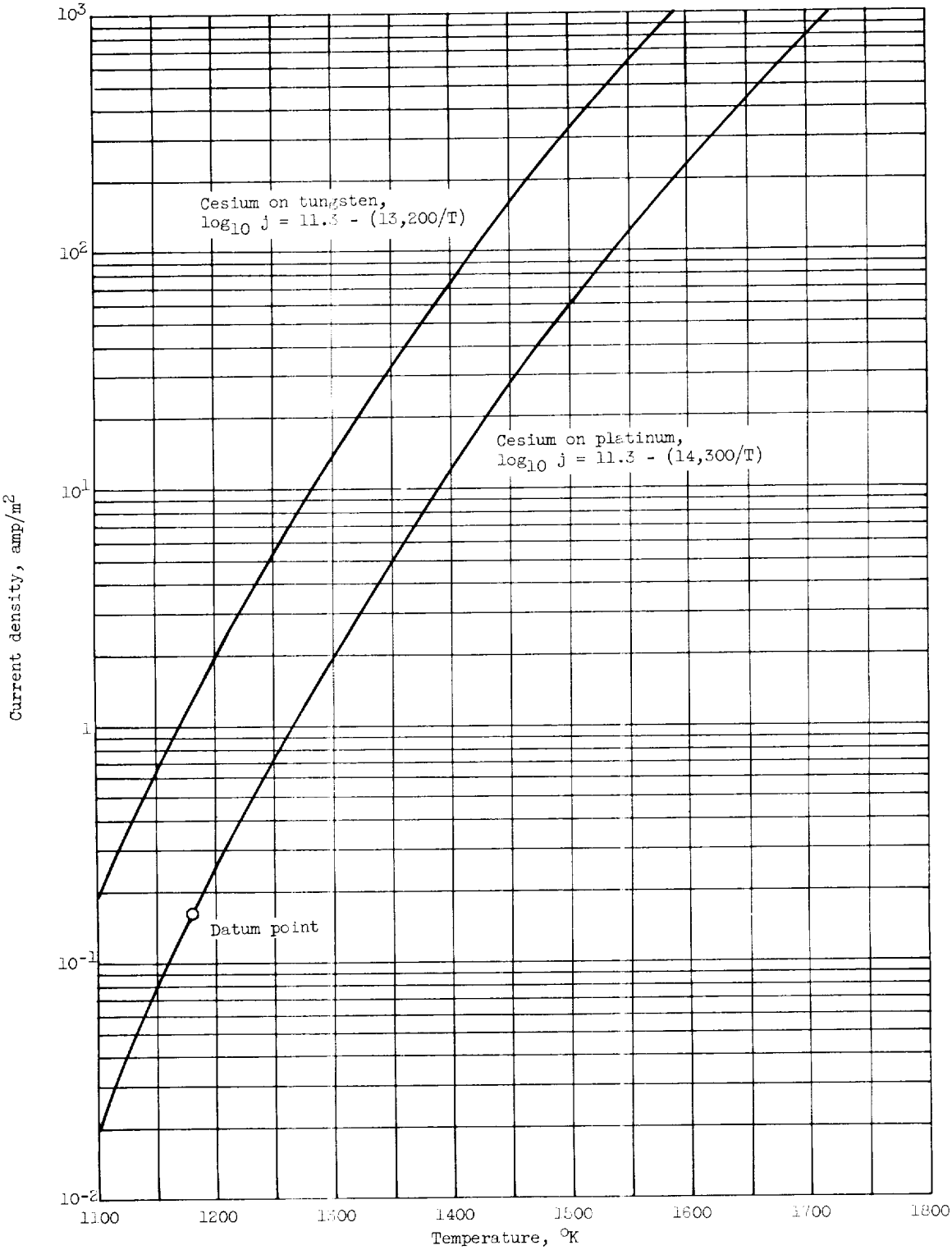

Figure 11. - Current - critical temperature relation for cesium on tungsten and platinum.

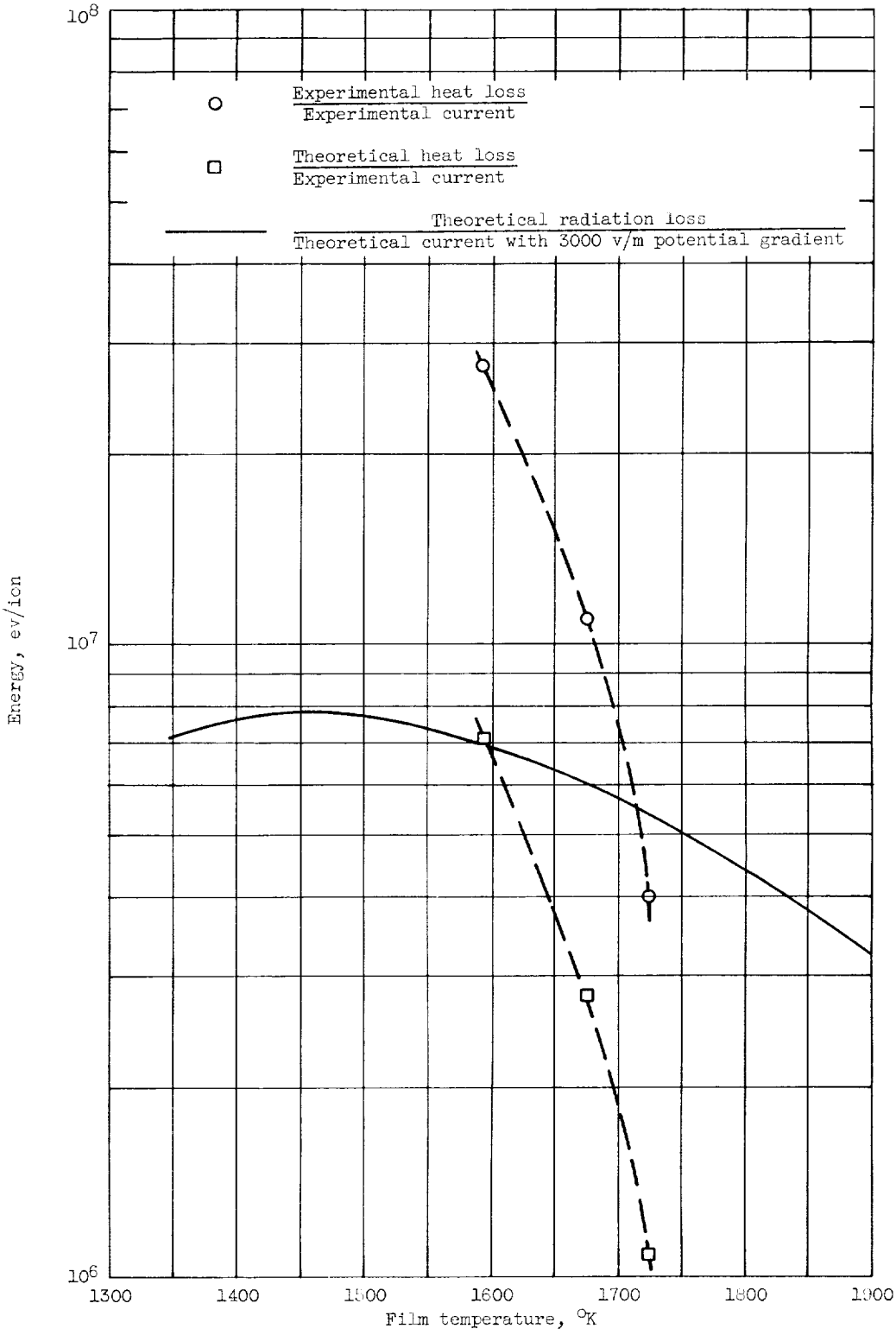

Figure 12. - Energy required to ionize atoms in cylindrical source with 3000-volt-per-meter longitudinal potential gradient.

E-1361